

# Formation of textured microstructure by mist deposition of TiO<sub>2</sub> nanoparticles

Gang Qin · Akira Watanabe

Received: 28 August 2013 / Accepted: 16 October 2013  
© Springer Science+Business Media Dordrecht 2013

**Abstract** Unique and various textured TiO<sub>2</sub> films have been easily fabricated by mist deposition method on silicon and glass substrates with mild preparation conditions. Two kinds of TiO<sub>2</sub> nanoparticle with different shape, size, and crystal form were used as starting material, which resulted in a simple preparation process under low temperature and ordinary pressure. It was easy to control the thickness, morphology, and roughness of textured TiO<sub>2</sub> film by adjusting the mist deposition conditions such as deposition time, temperature, and the shape and size of nanoparticles. The optical properties of textured TiO<sub>2</sub> films before and after spin coating of Ag nanoparticles were investigated. The angular dependence of the reflectance was obviously reduced by textured TiO<sub>2</sub> surface and such effect was enhanced by Ag nanoparticles coating. A broad plasmon band of Ag grains was observed in the absorption spectrum of the textured Ag nanoparticle-coated TiO<sub>2</sub> film.

**Keywords** Mist deposition · TiO<sub>2</sub> nanoparticle · Textured TiO<sub>2</sub> film · Surface texturing · Microstructure

## Introduction

TiO<sub>2</sub> film, which is a wide band gap (3.0–3.2 eV) and transparent oxide semiconductor, has potential applications in photocatalysis (Chen et al. 2007), solar cell (Tricoli et al. 2012), and sensor (Kim et al. 2008). The surface microstructure characteristics such as surface area, roughness, surface activity, and regularity play important roles in various properties, e.g., super-hydrophilicity (Gan et al. 2007), super-hydrophobicity (Lai et al. 2008), catalytic ability (Barrocas et al. 2013), and photoefficiency (Carnie et al. 2013). The variation of microstructure of thin film depends on the preparation methods and conditions, like evaporation (Duyar et al. 2008), sol–gel (Malengreaux et al. 2012), sputtering (Dhar and Alford 2013), electrophoretic method (Esquivel et al. 2011), plasma-enhanced chemical vapor deposition (Song et al. 2010), metal-organic chemical vapor deposition (Maekawa et al. 2008), and pulsed laser deposition (Dzibrou et al. 2008).

In previous paper, we have reported the novel technique for preparation of textured TiO<sub>2</sub> thin film using nanoparticles as starting material by mist deposition method (Qin and Watanabe 2013). This novel method offers advantages in terms of very simple

---

G. Qin · A. Watanabe (✉)  
Institute of Multidisciplinary Research for Advanced Materials, Tohoku University, Sendai 980-8577, Japan  
e-mail: watanabe@tagen.tohoku.ac.jp

G. Qin  
e-mail: qingang@tagen.tohoku.ac.jp

G. Qin  
School of Materials Science and Engineering, Henan Polytechnic University, Jiaozuo 454001, China

process and apparatus, low temperature without heat treatment, and so on. Especially, the morphology of the deposited film can be controlled conveniently owing to remarkably depending on the conditions such as kind of substrate, deposition time, substrate temperature, and nanoparticle shape and size.

In this paper, the influences of the deposition conditions on the morphology of the textured films were studied in detail to clarify the processes of surface texturing. As one of the applications of mist-deposited TiO<sub>2</sub> film, a textured reflector for a thin-film solar cell is expected because of the high reflective index of TiO<sub>2</sub>. For an efficient light trapping in the thin-film solar cell, the textured back reflector which will diffuse the light backward resulting in an increase in light path in the absorber layer is verified to be an effective technique to enhance photoelectric conversion efficiency (Hsu et al. 2012). If used as a reflector in solar cell, the mist-deposited film could diffuse the incident light due to the micro-textured structure. The reflectance and absorption properties of the mist-deposited film and the silver nanoparticle (Ag nanoparticle)-coated TiO<sub>2</sub> film (Ag/TiO<sub>2</sub> film) were investigated in comparison with a spin-coating TiO<sub>2</sub> nanoparticle film.

## Experiment

The schematic diagram of the mist deposition apparatus is shown in Fig. 1, which mainly consists of an atomizing system, a tube, and a heater chamber. Liquid precursors were TiO<sub>2</sub> nanoparticle suspensions prepared from TiO<sub>2</sub> nanoparticles (TK-535, rutile crystal form and TKS-201, anatase crystal form, Tayca Corp.) diluted by water to 0.06 mol/L. When the chamber and substrate were heated to given temperatures, the suspension was ultrasonically atomized and converted into a very fine mist which was then carried by nitrogen to the deposition chamber through a tube of 60 °C. The diameter of mist droplet was about 3 μm based on experimental data (Singh et al. 2008) when the frequency of the ultrasonic transducer was 2.5 MHz. P-type <100> silicon and glass substrates were used in our experiments, and before use the silicon substrate was irradiated by deep UV (Photo surface processor, PL16-110, Sen Light Corp.) for 20 min to introduce hydroxyl group on its surface in order to increase the hydrophilicity and to

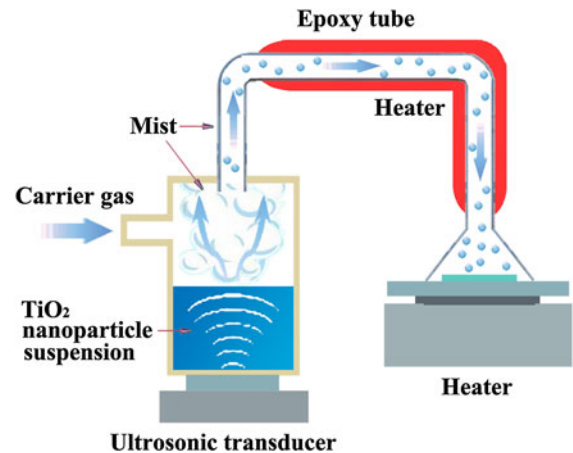


**Fig. 1** Reactor illustration for mist deposition method

improve the binding force of substrate/TiO<sub>2</sub> nanoparticles. The flow rate was controlled by a glass flowmeter. All the procedures were under 1 atm of pressure.

Ag nanoparticles with the diameter about 4 nm were applied in our experiments. The Ag nanoparticle ink (Ag1T, ULVAC, Inc.) was diluted with toluene to 1 wt%, and then spin-coated onto the mist-deposited TiO<sub>2</sub> film with the rotational speed of 2,000 rpm for 30 s at RT in air. The coated film was heated at 250 °C for 30 min to enhance the reflectance.

The surface morphology and thickness of the film were investigated using a violet laser scanning microscope (VK 9700, Keyence Corp.) and a scanning electron microscope (SEM, XL30, Philips Electronic N.V.). The reflectance was examined by the microscope with a ten times object lens and a CCD camera (DV401, Andor Technology) attached to a monochromator (MS257, Oriel Instruments Co.). The sample was put on the goniostage and the angle between the sample and incident light could be changed. The absorption spectrum was measured by a UV/Vis spectrophotometer (V-670DS, JASCO Corp.).

## Results and discussion

### Mist deposition process

Figure 2 shows the confocal optical micrographs and 3D images of ring structures prepared by mist deposition method with rutile TiO<sub>2</sub> nanoparticles as

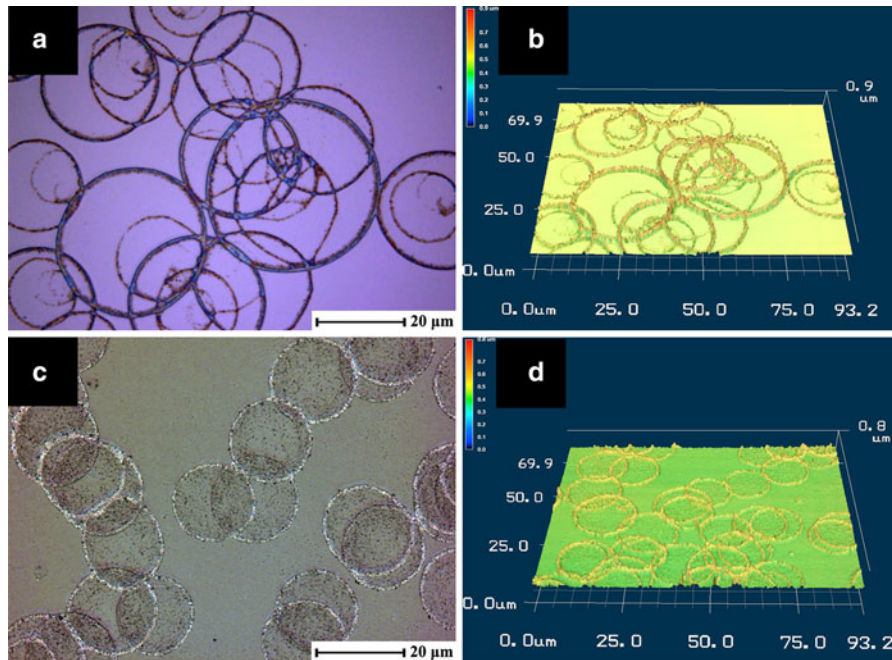


**Fig. 2** Ring structure prepared by mist deposition method observed by laser scan microscope (**a, b** silicon substrate; **c, d** glass substrate)

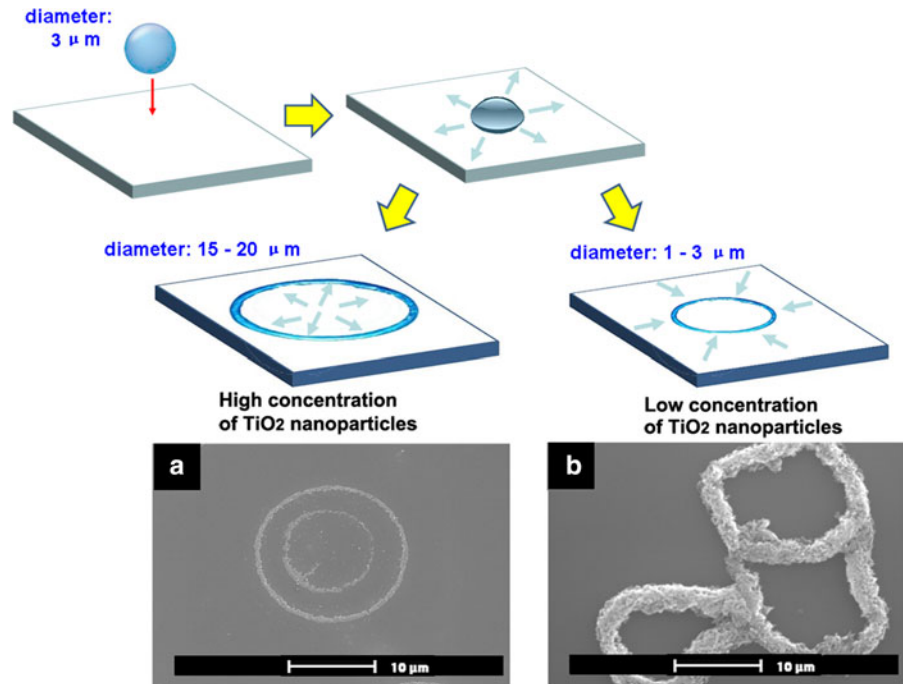
starting material on the silicon and the glass substrates, respectively. In the mist deposition of  $\text{TiO}_2$  nanoparticles, a ring structure was formed in the initial stage, which is the basic structural unit of textured  $\text{TiO}_2$  film. The process of the fabrication of the ring structure can be conjectured as illustrated in Fig. 3 as the result of the extension and flattening of the mist droplet after it deposited on the substrate. Because the evaporation of water from the flattened droplet occurred from the edge on a substrate, the water flow was caused from the center of the droplet to the edge. It also induced the transfer of the  $\text{TiO}_2$  nanoparticles from the drop point to the edge of the flattened droplet along the water flow, and then they would be fixed there by the interaction with the substrate.

With a high concentration dispersion of  $\text{TiO}_2$  nanoparticles around 0.06 mol/L, the rings are regular with the diameter around 15–20  $\mu\text{m}$  as demonstrated in Fig. 3a. However, when the concentration decreases to 0.01 mol/L, the rings become irregular and the diameter reduces to 1.13–3.02  $\mu\text{m}$  as indicated in Fig. 3b. In addition, a connected ring structure is observed in the mist deposition with low concentration  $\text{TiO}_2$  dispersion. In this case, it was difficult for the nanoparticles to aggregate and the interaction between

substrate and nanoparticles was low on the edge of the flattened droplet, which caused the return flow of  $\text{TiO}_2$  nanoparticles from the edge to the drop point with shrinkage of the flattened droplet. The overlapping of the contractive droplets formed the connected ring structure as shown in Fig. 3b. Additional feature of the ring structure as shown in Fig. 3a is the concentric circle structure. The inner ring must be formed during the return flow of droplet after the aggregation of almost  $\text{TiO}_2$  nanoparticles at the outer edge.

The influences of the substrate presented in Fig. 2 can be explained by considering the mechanism of ring formation discussed above. It is apparent that there are many dots in the rings on the glass substrate; on the contrary, for the silicon substrate the surface is clean in the range of rings. Such distinction can be explained by the different interaction between  $\text{TiO}_2$  nanoparticles and substrate depending on the hydrophilicity of the substrate surface, which is mainly caused by the hydroxyl groups on it. By this reason, the interaction between  $\text{TiO}_2$  nanoparticles and the glass substrate with more hydroxyl groups is stronger than that in the case of the silicon substrate with fewer hydroxyl groups, corresponding to some nanoparticles remain on the glass substrate during the extension of

**Fig. 3** The process of mist deposition with TiO<sub>2</sub> nanoparticles (**a** 0.06 mol/L; **b** 0.01 mol/L)



droplet, as shown in Fig. 2c. The size distribution of the ring is narrow as shown in Fig. 2, which is due to the uniformity of the mist size depending largely on the frequency of a transducer.

#### Influence of deposition time

The change of surface morphologies of deposited TiO<sub>2</sub> film with time was captured by SEM as shown in Fig. 4, and the thicknesses and the root mean square roughnesses (RMS) of every film are listed in Table 1. At the beginning of mist deposition process, only several separated rings could be observed, the thickness of which is about 69–126 nm, and the diameter is in the range of 14.35–20.16 μm (Fig. 4a). With deposition time increasing to 5 min, a network formed by some crossed lines as illustrated in Fig. 4b with the thickness of 0.26 μm, the width of the lines of 1.02 μm and RMS of 0.068 μm. If time continued to increase to 10 min, as a result of the overlapping of the rings, uneven size pores and rough textured surface were formed by the crossed lines like veins (Fig. 4c). The depth of the pores is 0.43–0.62 μm and the diameter is estimated to be 2.46–8.21 μm. The thickness of the film is approximately 1.36 μm, the width of vein is about 2.04 μm, and RMS is 0.42 μm. The thickness of the textured TiO<sub>2</sub> film whose surface covered by pores

and networks increases approximately to 3.27 μm after a deposition time of 15 min (Fig. 4d). Namely, the longer the deposition lasts, the more the particles reach the substrate. The depth and the diameter of the pores are close to Fig. 4c, while the vein width increases to 2.89 μm and the RMS 0.47 μm. With further prolongation of the deposition time to 30 min (Fig. 4e), the pore structure disappeared due to the filling of excess nanoparticles and a flat film was obtained with the thickness up to 10.62 μm. The line roughnesses of the samples with different deposition time are illustrated by the graph in Fig. 5. At the initial stage, there are some vertical salient parts corresponding to the wall of separated rings as shown in Fig. 5a; the thickness and roughness increased with the time extension, so the height difference increases and the roughness curve becomes more crooked as exhibited in Fig. 5b, c, d; after long deposition time, the curve in Fig. 5e becomes smooth because textured structure was filled by nanoparticles and the roughness decreased.

#### Influence of temperature

Figure 6 exhibits the dependence of the morphology and thickness of the film on the substrate temperature during mist deposition. The results indicate that the thickness of the film increased from 0.18 to 3.74 μm

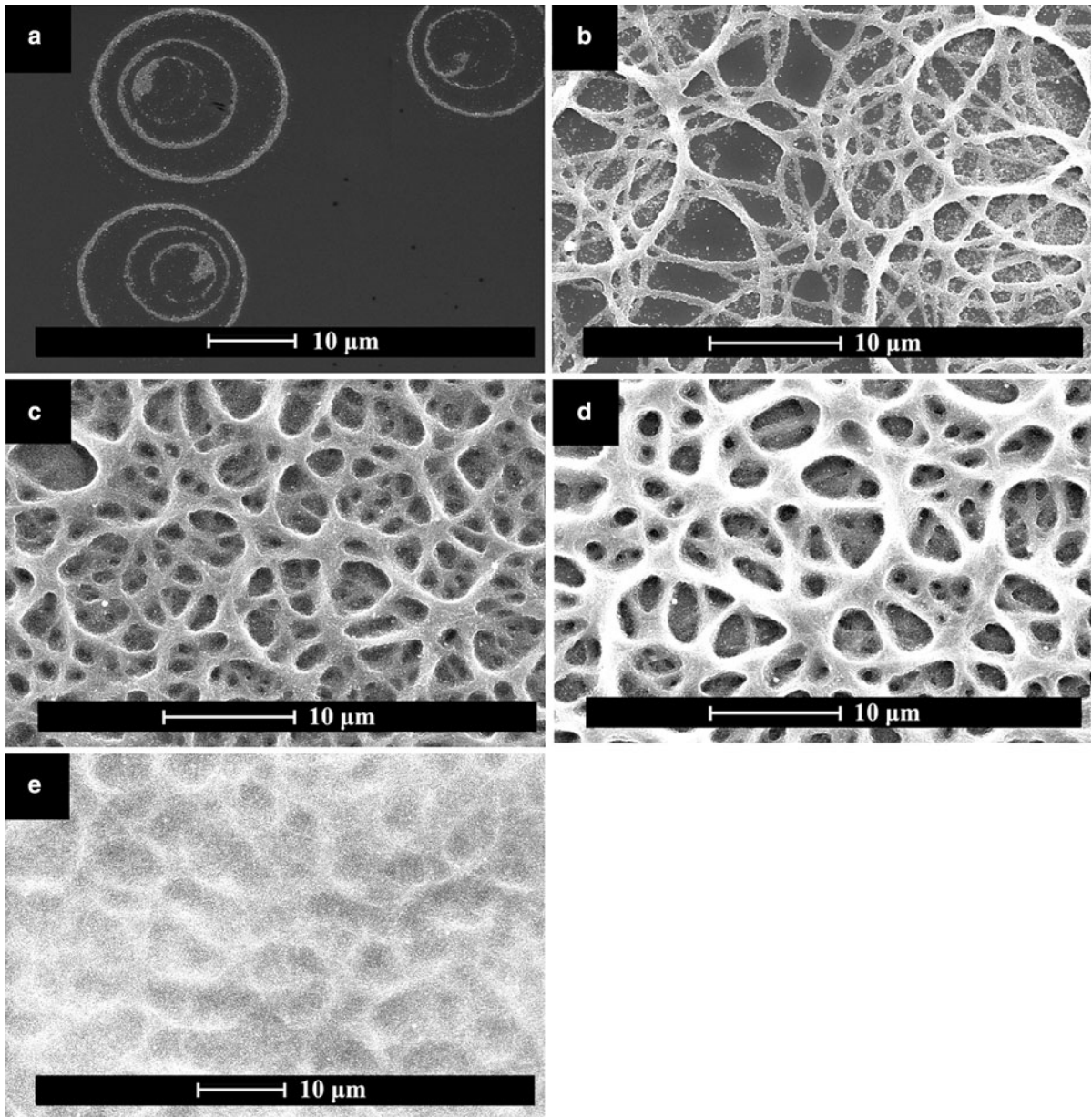


**Fig. 4** SEM images of the  $\text{TiO}_2$  films prepared with different deposition time by mist deposition method (conditions: rutile nanoparticle, 0.06 mol/L, 100 °C, 1 L/min, silicon substrate. **a** 1 min; **b** 5 min; **c** 10 min; **d** 15 min; **e** 20 min)

and the width of veins from 1.22 to 2.89  $\mu\text{m}$  with the temperature decreasing from 200 to 80 °C. The interpretation of this result could be the upward airflow from the heated substrate. When the substrate temperature was higher than the boiling point, it was difficult for the mist to deposit on the substrate because of the stronger upward vapor flow from the

substrate. The thinner film as shown in Fig. 6d was resulted from the difficult deposition at the higher temperature. On the contrary, the decrease in the substrate temperature obviously brought about thicker film and affected the morphology, for example, the film porosity decreasing, due to the arrival of many more particles to the substrate.

**Table 1** Thickness and RMS of the TiO<sub>2</sub> films prepared with different deposition time by mist deposition method

Deposition time (min)	Thickness (μm)	RMS (μm)
1	0.069–0.13	0.036
5	0.26	0.068
10	1.36	0.42
15	3.27	0.47
30	10.62	0.193

Conditions: rutile nanoparticle, 0.06 mol/L, 100 °C, 1 L/min, silicon substrate

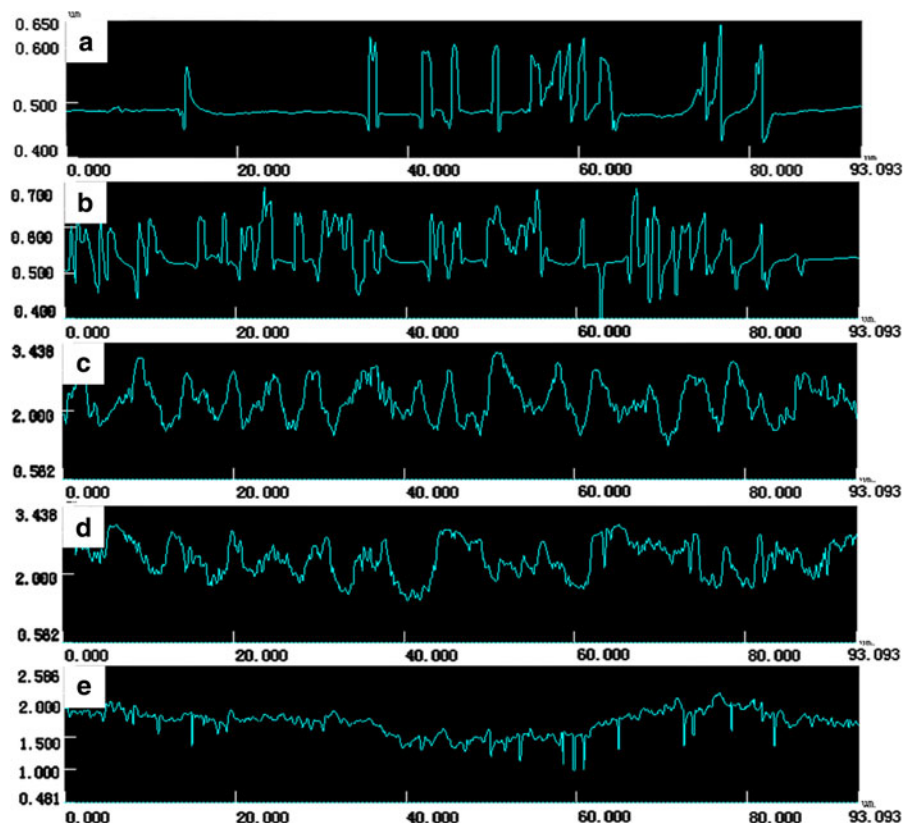
### Influence of nanoparticle shape and size

The morphologies of two kinds of TiO<sub>2</sub> nanoparticle were investigated through SEM and their shapes and sizes are quite different as indicated in Fig. 7g, h. The rutile TiO<sub>2</sub> (TK-535) is in rod-like form having a length of 80 nm and a width of 30 nm, on the other hand, the anatase TiO<sub>2</sub> (TKS-201) is cubic with the length of every side about 40 nm measured by SEM images, such rod-like (Sonawane and Ramakrishna 2012) and

cubic (Pan et al. 2011) crystals have been reported previously. As illustrated in Figs. 7a, b, e, f, there are remarkable differences of microstructures on the films fabricated with two kinds of nanoparticle. Under the same deposition conditions, the film prepared from the rutile nanoparticles is thicker than the one from the anatase nanoparticles (2.33 μm) and the vein of the former is also wider than the latter (2.05 μm). The difference in the line width of networks is also evident as shown in Fig. 7e, f. The line width of the networks fabricated from the anatase nanoparticles is about 0.21–0.78 μm. The detail images of the morphologies of rings and textured films are depicted in Fig. 7c, d, g, h. Most of rutile nanoparticles align along the long-axis direction and the anatase nanoparticles are closely packed, indicating that the microstructures were formed by the aggregation and ordered arrangement of nanoparticles. The aggregation of some rod-like rutile nanoparticles looks like aligning along the flow from the center to the edge of the droplet.

The differences of the tendency in the film morphologies that the film of rutile TiO<sub>2</sub> nanoparticles is thicker and the vein is wider may be

**Fig. 5** Roughness of the TiO<sub>2</sub> films prepared with different deposition time by mist deposition method (conditions: rutile nanoparticle, 0.06 mol/L, 100 °C, 1 L/min, silicon substrate. **a** 1 min; **b** 5 min; **c** 10 min; **d** 15 min; **e** 20 min)



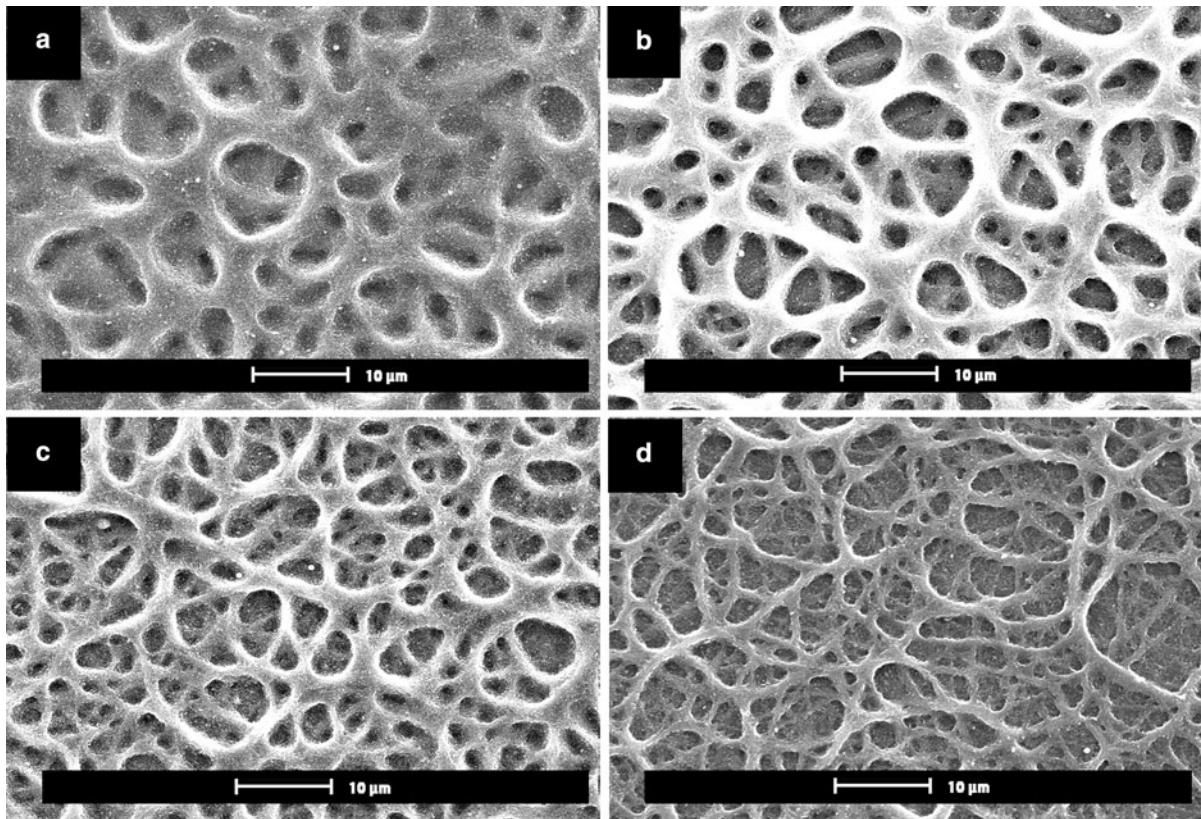


**Fig. 6** SEM images of the TiO<sub>2</sub> films prepared at different substrate temperature by mist deposition method (conditions: rutile nanoparticle, 0.06 mol/L, 15 min, 1 L/min, silicon substrate. **a** 80 °C, **b** 100 °C, **c** 150 °C, **d** 200 °C)

predominantly attributed to the size and shape of nanoparticles. The aggregation of the larger rutile nanoparticles is easier to occur than that of the smaller anatase nanoparticles in our experiments, and the aggregated nanoparticles can be fixed at the fringe of the droplet. Another possible reason is that the shape of anatase nanoparticle is cubic, which results in easier rotation and movement during the deposition process (Venerus et al. 2010) compared to rod-like rutile nanoparticle.

### Optical properties

We have shown that the textured TiO<sub>2</sub> surface morphology can be simply controlled by changing deposition conditions and nanoparticle shape and size. In the following, the optical properties of the textured TiO<sub>2</sub> film were investigated. As an important property in the application to a reflector, the angular dependence

of the reflectance was discussed using the normalized reflectance ( $R_{NR}$ ) defined as follows.

$$R_{NR}(\lambda) = \frac{R_{\theta}(\lambda)}{R_{ref}(\lambda)}$$

where  $\lambda$  is the wavelength of incident light,  $R_{ref}(\lambda)$  is the intensity of reflected light when the surface is perpendicular to the incident light and  $R_{\theta}(\lambda)$  is the intensity of reflected light when the incident angle is  $\theta$  adjusted by a gonio-stage.

The angular dependences of  $R_{NR}$  of glass, spin-coating TiO<sub>2</sub> film and textured TiO<sub>2</sub> film are shown in Fig. 8a when the wavelength of incident light is 600 nm. The  $R_{NR}$ s of glass and spin-coating TiO<sub>2</sub> nanoparticle film are quite sensitive to the incident angle. The  $R_{NR}$ s decrease very fast with increasing the incident angle, and they, respectively, drop to 0.33 and 0.52 % on glass and spin-coating TiO<sub>2</sub> film at 10°, which indicates the weak diffusion phenomenon on

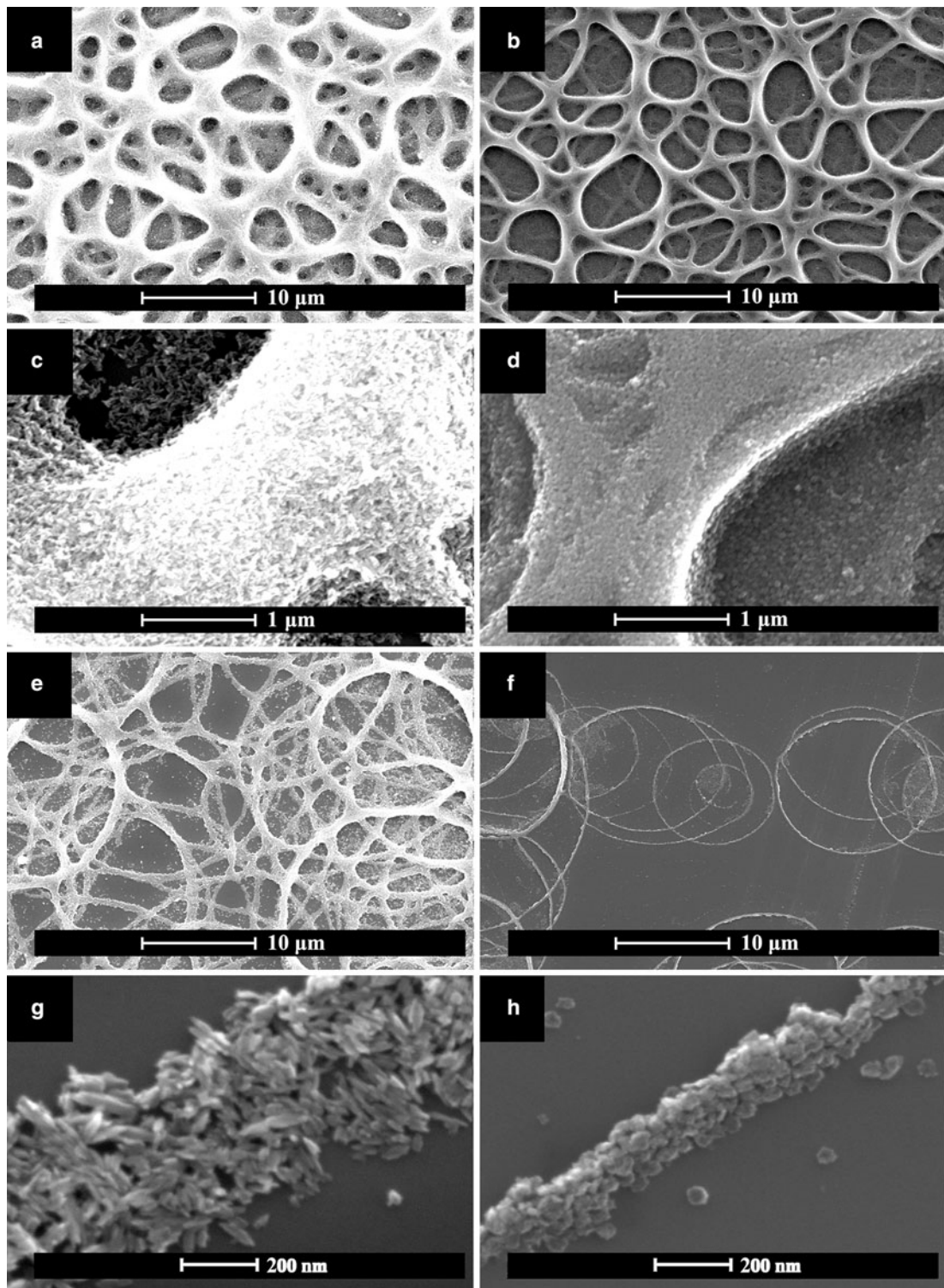
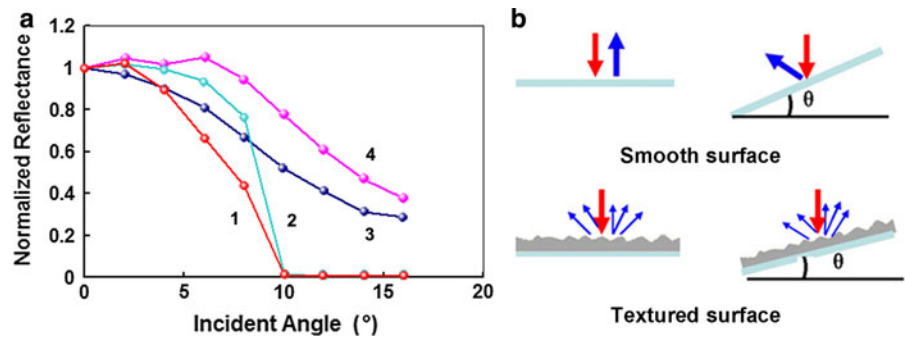


**Fig. 7** SEM images of TiO<sub>2</sub> films prepared by mist deposition method with rutile (**a**, **c**, **e**, and **g**) and anatase (**b**, **d**, **f**, and **h**) TiO<sub>2</sub> nanoparticles (conditions: rutile and anatase TiO<sub>2</sub> nanoparticles, 0.06 mol/L, 100 °C, 15 min, 1 L/min, silicon substrate)

**Fig. 8** Angular dependence of reflectance of textured TiO<sub>2</sub> and Ag/TiO<sub>2</sub> film. (1 glass; 2 spin-coating TiO<sub>2</sub> film; 3 mist-deposited TiO<sub>2</sub> film; 4 Ag/TiO<sub>2</sub> film. conditions: rutile nanoparticle, 0.06 mol/L, 100 °C, 15 min, 1 L/min, glass substrate)



the smooth surface. On the contrary, the textured TiO<sub>2</sub> film represents the low angular dependence compared to the glass and spin-coating TiO<sub>2</sub> nanoparticle film. The  $R_{NR}$  is still about 35 % at 16°, whereas the  $R_{NR}$ s of the smooth surfaces become almost zero around 10°. These results suggest the diffusion on the textured surface occurred remarkably as illustrated in Fig. 8b.

The coating of Ag nanoparticles on the textured TiO<sub>2</sub> film surface was investigated so as to improve the reflectance properties. The Ag nanoparticle ink (1 wt%, toluene suspension) was spin-coated onto the mist-deposited TiO<sub>2</sub> film and then the film was heated at 250 °C for 30 min. The sintering of the Ag nanoparticles enhanced the reflectance because the nanoparticles fused and then formed a metallic phase accompanying the decomposition of organic groups stabilizing the Ag nanoparticles. As shown in Fig. 8a, the angular dependence was further reduced due to the higher reflectance by covering the textured TiO<sub>2</sub> film with the Ag layer. The high diffuse reflectance of these samples is beneficial for the potential of application as a reflector.

It is well known that Ag nanoparticles show characteristic absorption spectrum attributed to the plasmon band in visible region. In the case of a spin-coating film of Ag nanoparticle ink on a smooth glass substrate, the plasmon band disappeared by heating due to the fusion and the formation of continuous Ag layer. The absorption spectra of the textured TiO<sub>2</sub> film before and after Ag covering and the spin-coating TiO<sub>2</sub> film were measured to investigate the structure of heat treated Ag nanoparticles on the textured TiO<sub>2</sub> film. As to spin-coating TiO<sub>2</sub> film, there is a weak absorption in visible region due to its high transparency as shown in Fig. 10a.

The textured TiO<sub>2</sub> film exhibits a broad absorption in the whole wavelength region, however, it should be

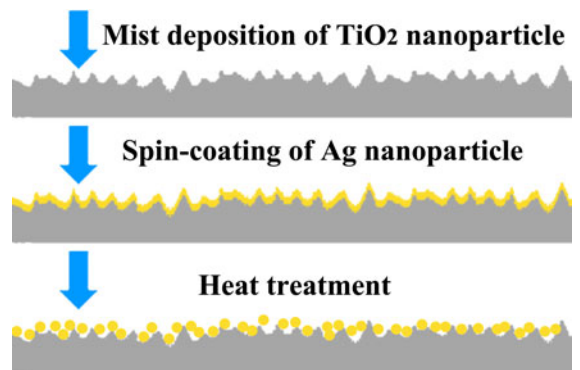


**Fig. 9** Process of Ag/TiO<sub>2</sub> film preparation

due to apparent absorption caused by the light diffusion on the textured surface. The band around 380 nm may be due to the light interference in the textured film. With Ag nanoparticle coating, the textured TiO<sub>2</sub> film appeared red color owing to the plasmon band, and the color faded but remained partly after sintering at 250 °C. In the absorption spectrum of the textured Ag/TiO<sub>2</sub> film, a broad absorption band appears in 350–560 nm spectral range, which can be assigned to plasmon band of Ag nanoparticles. Although the absorption peak around 460 nm is almost the same as that of Ag nanoparticle film without heat treatment, the noticeable broadening of the absorption spectrum of the textured Ag/TiO<sub>2</sub> film suggests that there are Ag grains with various sizes by fusion of Ag nanoparticle aggregates existing separately in the macro-pore of the textured TiO<sub>2</sub> film even after the heat treatment as illustrated in Fig. 9, which is confirmed by the SEM image of the textured Ag/TiO<sub>2</sub> film (Fig. 10b). The enhancement of the  $R_{NR}$  as exhibited in Fig. 8 must be caused by such Ag grains fixed into the macro-pore of the textured TiO<sub>2</sub> film.

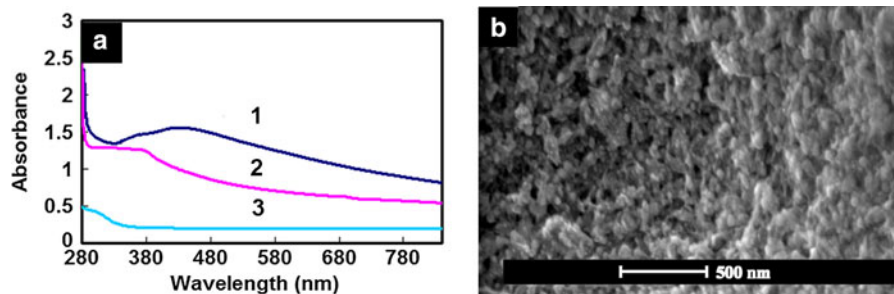


**Fig. 10** Absorption spectra and SEM image of textured Ag/TiO<sub>2</sub> film. (1 Ag/TiO<sub>2</sub> film; 2 mist-deposited TiO<sub>2</sub> film; 3 spin-coating TiO<sub>2</sub> film. Conditions: rutile nanoparticle, 0.06 mol/L, 100 °C, 15 min, 1 L/min, glass substrate)

## Conclusion

Using TiO<sub>2</sub> nanoparticles as starting material, porous and textured thin films with unique and various microstructures were simply and effectively fabricated by mist deposition method at low temperature and ordinary pressure. The thickness and morphology of the film can be easily controlled by changing the conditions such as deposition time, temperature, and nanoparticle shape and size. The angular dependence of the reflectance was reduced by textured TiO<sub>2</sub> surface and such effect was enhanced by Ag nanoparticle coating. A broad plasmon band of Ag grains can be observed in the absorption spectrum of the textured Ag/TiO<sub>2</sub> film after heat treatment.

**Acknowledgments** This work was supported by a Grant-in-Aid for Scientific Research on Innovative Areas “New Polymeric Materials Based on Element-Blocks (No.2401)” (24102004) of The Ministry of Education, Culture, Sports, Science, and Technology, Japan.

## References

- Barrocas B, Monteiro OC, Melo Jorge ME, Sério S (2013) Photocatalytic activity and reusability study of nanocrystalline TiO<sub>2</sub> films prepared by sputtering technique. *Appl Surf Sci* 264:111–116
- Carnie MJ, Charbonneau C, Barnes PRF, Davies ML, Mabbett I, Watson TM, O'Regard BC, Worsley DA (2013) Ultra-fast sintered TiO<sub>2</sub> films in dye-sensitized solar cells: phase variation, electron transport and recombination. *J Mater Chem A* 1:2225–2230
- Chen CC, Bai HL, Chang SM, Chang CL, Den W (2007) Preparation of N-doped TiO<sub>2</sub> photocatalyst by atmospheric pressure plasma process for VOCs decomposition under UV and visible light sources. *J Nanopart Res* 9:365–375
- Dhar A, Alford TL (2013) High quality transparent TiO<sub>2</sub>/Ag/TiO<sub>2</sub> composite electrode films deposited on flexible substrate at room temperature by sputtering. *APL Mater* 1:012102
- Duyar Ö, Placido F, Durusoy ZH (2008) Optimization of TiO<sub>2</sub> films prepared by reactive electron beam evaporation of Ti<sub>3</sub>O<sub>5</sub>. *J Phys D* 41:095307
- Dzibrout D, Grishin AM, Kawasaki H, Suda Y, Pankov VV (2008) Tailoring optical properties of pulsed laser deposited TiO<sub>2</sub> films. *J Phys* 100:082035
- Esquivel K, MG Garcí'a J, Rodríguez FJ, Gonza'lez MV, Escobar-Alarco'n L, Ortiz-Frade L, Godí'nez LA (2011) Titanium dioxide doped with transition metals (MxTi1-xO<sub>2</sub>, M: Ni, Co): synthesis and characterization for its potential application as photoanode. *J Nanopart Res* 13:3313–3325
- Gan WY, Lam SW, Chiang K, Amal R, Zhao H, Brungs MP (2007) Novel TiO<sub>2</sub> thin film with non-UV activated superwetting and antifogging behaviours. *J Mater Chem* 17:952–954
- Hsu CM, Battaglia C, Pahud C, Ruan Z, Haug FJ, Fan S, Ballif C, Cui Y (2012) High-efficiency amorphous silicon solar cell on a periodic nanocone back reflector. *Adv Energy Mater* 2:628–633
- Kim DI, Rothschild A, Yang DJ, Tuller HL (2008) Macroporous TiO<sub>2</sub> thin film gas sensors obtained using colloidal templates. *Sens Actuators B* 130:9–13
- Lai YK, Lin CJ, Huang JY, Zhuang HF, Sun L, Nguyen T (2008) Markedly controllable adhesion of superhydrophobic sponge-like nanostructure TiO<sub>2</sub> films. *Langmuir* 24:3867–3873
- Maekawa T, Kurosaki K, Tanaka T, Yamanaka S (2008) Thermal conductivity of titanium dioxide films grown by metal-organic chemical vapor deposition. *Surf Coat Technol* 13:3067–3071
- Malengreuxa CM, Timmermans A, Pirarda SL, Lamberta SD, Pirarda JP, Poelman D, Heinrichs B (2012) Optimized deposition of TiO<sub>2</sub> thin films produced by a non-aqueous sol-gel method and quantification of their photocatalytic activity. *Chem Eng J* 195–196:347–358
- Pan J, Liu G, Lu GQ, Cheng HM (2011) On the true photoreactivity order of {001}, {010}, and {101} facets of anatase TiO<sub>2</sub> crystals. *Angew Chem Int Ed* 50:2133–2137
- Qin G, Watanabe A (2013) Surface texturing of TiO<sub>2</sub> film by mist deposition of TiO<sub>2</sub> nanoparticles. *Nano-Micro Lett* 5:129–134
- Singh P, Kumar A, Deepak Kaur D (2008) ZnO nanocrystalline powder synthesized by ultrasonic mist-chemical vapour deposition. *Opt Mater* 30:1316–1322

- Sonawane RS, Ramakrishna S (2012) Facile method for the selective growth of rice like rutile TiO<sub>2</sub> from peroxotitanate gel and its photo-activity. *Mater Sci Eng B* 177:652–660
- Song SJ, Park YJ, Park J, Cho MD, Kim JH, Jeong MH, Kimc YS, Cho DL (2010) Preparation of a drug-eluting stent using a TiO<sub>2</sub> film deposited by plasma enhanced chemical vapour deposition as a drug-combining matrix. *J Mater Chem* 20:4792–4801
- Tricoli A, Walleranda A, Righettonia M (2012) Highly porous TiO<sub>2</sub> films for dye sensitized solar cells. *J Mater Chem* 22:14254–14261
- Venerus DC, Buongiorno J, Christianson R (2010) Viscosity measurements on colloidal dispersions (nanofluids) for heat transfer application. *Appl Rheol* 20:44582